Institute of Space and Aeronautical Science, University of Tokyo
Report No. 403, June 1966

Instruments for the Observation of Garactic X-Rays

By

Masaru MATSUOKA

Summary. Three types of rocket-borne X-ray instruments were constructed; they consist of a scintillation counter, four proportional counters and twenty-three GM counters respectively. The scintillation counter was used to observe isotropic X-rays in the energy ranges of 5~10, 10~15, 15~20 and $\geq$20 KeV, and the proportional counters to observe the intensities of X-rays from several sources in the energy ranges of 2~4, 4~8 and 8~16 KeV. The GM counters were used to observe the intensities of X-rays from several sources in the wavelength ranges of 2~4, 4~8 and 7~11 Å. Their properties were tested by radioactive sources and were found to be suitable to analyze the energy spectrum of galactic X-rays and to reject charged particles. Their counter systems were successful to obtain several data of galactic X-rays and atmospheric X-rays, and the method of data analyses as well as preliminary results are also described.

1. INTRODUCTION

The observation of extra-terrestrial X-rays has put conspicuous interest, since the discovery of X-ray emission outside the solar system (refer to as galactic X-rays) by Giacconi et al in 1962 [*1*]. Since then X-ray astronomy has been recognized as an important field of modern astrophysics.

Galactic X-rays are emitted from a number of local sources; and their intensities are unexpectedly large. It is very difficult to understand the nature of the X-ray sources and their intensities from our normal concept in astrophysics. In order to go one step farther detailed observations with various methods are required for clarifying their strong intensities, emission mechanisms in their sources, the structure of X-ray sources and so on.

We have constructed several instruments for the observation of galactic X-rays with Japanese sounding rocket, and results obtained thereby have offered a number of important results. Since our brief reports were published [*2*, *3*, *4*], and results of detailed analyses will be presented in separate papers, we describe instruments for the observation of galactic X-rays in the present paper; properties of detectors, functions of each instrument and the method of data analysis are the main subject in our discussion.

In 2 we discuss the importance of X-ray astronomy together with its historical review as well as the general description of instruments.

In 3 we describe the performance of the scintillation counter, the proportional

counter and the GM counter which we used to observe X-rays with rockets.

4 is spent for discussions of the electronic system by which pulses from detectors are treated.

In 5 we consider the method of data analysis. From counting rates observed we were able to deduce the absolute intensities and spectral shapes of X-rays concerned.

In 6 we summarize our rocket-borne instruments and results of observations.

2. General Description of Galactic X-Rays

Since X-rays are subject to absorption in the atmosphere, one must go outside the atmosphere or to a very high altitude to observe galactic X-rays. For this purpose X-ray detectors have to be constructed so as to be suitable for balloon-, rocket- or satellite-borne.

Observations of galactic X-rays have thus far been performed mainly with rockets by ASE-MIT [*5*], NRL [*6*, *7*], Lockheed [*8*] and Nagoya groups [*2*, *3*, *4*], and their results are summarized as follows.

i) About ten and several X-ray sources have been discovered.
ii) Most of X-ray sources are concentrated in the Galactic disk.
iii) A few of them are identified with optical and raidio sources, that is, Tau A, Cyg A, Cas A and M 87.
iv) The X-ray source of the Crab nebula was measured to have the angular size as large as one minute of arc by means of the lunar occultation [*9*].
v) An upper limit of 20 seconds of arc on the diameter of Sco X-1 has been measured with a modullation collimator [*10*].
iv) The angular sizes of other X-ray sources seem to be less than half a degree.
vi) The angular sizes of other X-ray sources seem to be less than half a degree.
vii) The flux intensities from respective sources are as strong as 0.2 to 20 photons $cm^{-2}sec^{-1}$ in the wavelength region between 2 and 8 Å.
viii) The spectra of most of sources seem to fall off sharply beyond 20 KeV, but the X-ray spectrum of Crab nebula is extended to high energy region.
ix) The isotropic intensity of galactic X-rays is about 6 photons $cm^{-2}sec^{-1}sr^{-1}$ at the wavelength of 2~8 Å.

Our observations gave several new results such as the energy spectrum of isotropic X-rays and those of some local suorces. In this paper, however, we do not discuss astrophysical implications of the results, but only refer to our earlier paper [*11*] about a general scope as well as to our future papers concerning respective experiments.

In our experiments we used a scintillation counter, proportional counters and GM counters which were representative X-ray detectors thus far employed by other groups [*12*] as well. These three types of counters are rather easy to use as instruments for rocket observation, but they must be constructed so as to work under the severe environment of rockets which are subjected to violent vibration, strong shock, vacuum and so on.

TABLE I. Properties of X-ray counters for galactic X-rays.

Counter		Properties: Gas filled (pressure)	Properties: window material (area of each)	Properties: acceptance angle (half maximum)	Angular between a counter and a rocket axis	X-ray energy (or wavelength) range	Telemeter response frequency
Scintillation counter		—	150 μ Be (4.52 cm^2)	±82° (±51°)	45°	I 5~10 KeV II 10~15	45 c/s
						III 15~20 IV ≥20	35
Proportional counter		Xe (320 mmHg)	100 μ Be (3.27 cm^2)	±45° (±20°)	75° and 105°	I 2~ 4 II 4~ 8	220
						III 8~16 IV ≥16	100
GM counter	GMI	Ar (750 mmHg)	100 μ Be (4.7 cm^2)	±20° (±8.5°)	90°	1~3.8Å 3.8~8	330
	GMII	Ne (700 mmHg)	100 μ Be (4.7 cm^2)	±20° (±8.5°)	90°	2~8	220
	GMIII	Ne (700 mmHg)	3.3 μ Mica (2.5 cm^2)	±20° (±8.5°)	90°	2~7.4 7.4~11	160

Table I shows various properties of X-ray counters used for our observations of galactic X-rays. Several counters were used except in the first flight with one scintillation counter. This is necessary for increasing the detection area; the detection area of one counter can not be increased too much, because of the difficulty in making the window too large with transparent but brittle materials. A cylindrical collimator made of a plastic material was attached to each counter, but the acceptance angle and the full width at half maximum which were extended to rather wide angles are rather large, becouse otherwise the X-ray counting rate would become too low. These counters were attached to the main stages of rockets with suitable angles with the rocket axis.

Our scintillation counter was stable and was able to offer a spectrum of isotropic X-rays in the energy range of 5~20 KeV. Proportional counters and GM counters were suffered from an age effect, because they were sealed off gas counters, but we calibrated properties of counters just before rocket flights.

Sky regions scanned were determined with the aid of rocket trajectories and the geomagnetic aspectmeters. Counting rates in respective energy regions were telemetered by the FM-FM method with response frequencies listed in Table I and recorded by reference to time and geomagnetic aspect.

3. X-RAY COUNTERS

In order to examine properties of counters some calculations and experiments were carried out. Here we describe some problems common to three types of

counters.

The counting efficiency of counters for an X-ray of an energy k is obtained from the expression

$$\varepsilon(k)=e^{-\{\mu(k)\rho X\}w}\left[1-e^{-\{\mu(k)\rho X\}s}\right], \qquad (1)$$

where μ is the mass absorption coefficient, ρ the density and X the effective thickness, the quantity with suffix w indicates the absorption in the window and the quantity with suffix s that in the scintillator or the counter gas.

Various properties of counters were examined by using radioactivities of ^{55}Fe, ^{65}Zn and ^{109}Cd, which emit K X-rays of 5.9, 8.04 and 22.1 KeV respectively. ^{109}Cd also emits a γ-ray of 88 Kev and other weak contaminating radiations. γ-rays from ^{137}Cs and β-rays from ^{147}Pm and ^{90}Sr were used for testing effects of contaminating radiations. Pulse height distributions due to radiations from those radioactive sources were analyzed by a TMC 400 channels pulse height analyzer. The radiations were collimated through a hole of a few millimeters diameter which was set at a distance of several centimeters from the counters. Energies and approximate intensities of the radiations used are listed in Table II.

TABLE II. Radioactivities used for testing properties of counters.

Elements	Radiation (energy)	Approximate intensities
^{55}Fe	X-ray (5.9 KeV)	10 μC
^{65}Zn	〃 (8.04 KeV)	〃
^{109}Cd	〃 (22.1, 88 KeV)	〃
^{137}Cs	γ-ray (662 KeV	100 μC
	β-ray (514 KeV, max)	
^{147}Pm	β-ray (227 KeV, max)	〃
^{90}Sr	β-ray (545 KeV, max)	1 μC

For isotropic X-rays it is required to introduce a geometrical factor G as a product of the effective area and the solid angle. If the efficiency concerned does not depend on the incident angle, it can be calculated in consideration of geometrical configurations. Taking into account that the cylindrical collimators of these counters have lengths of 3.3, 20 and 30 mm, we obtain

$G=S\Omega=10.7$ cm^{2}sr for a scintillation counter,
〃 $=1.24$ 〃 for a proportional counter,
〃 $=0.33$ 〃 for a GM counter of type I or II,
〃 $=0.16$ 〃 for a GM counter of type III.

3.1. SCINTILLATION COUNTER

A scintillation counter has been used to detect X-rays with energies of several KeV and greater in various fields of research. We have employed this detector in our first observation of galactic X-rays. In Fig. 1 is shown the scintillation counter which was borne on a Japanese sounding rocket named as L-3-3. This counter was

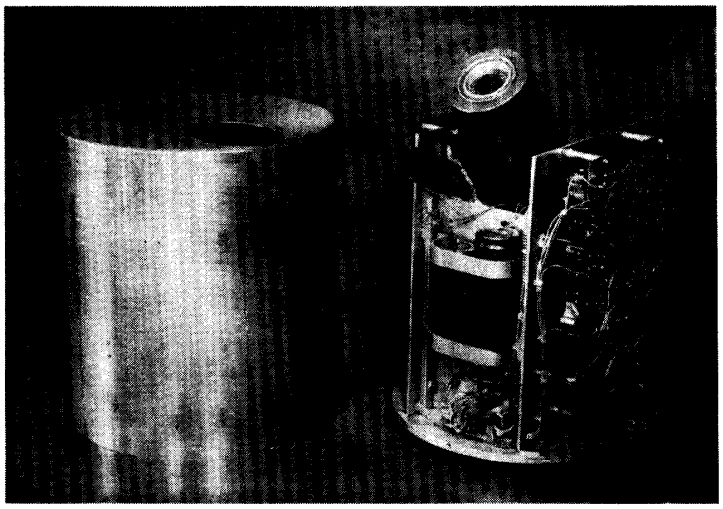

FIG. 1. The Scintillation counter borne on the rocket, L-3-3.

put at the top of the nose cone of the rocket, so that background radiations produced from materials of environment are reduced to be as weak as possible.

1. Counting efficiency of a scintillator

Our scintillator was a block of NaI(T1)*) of 25×1.5 mm whose fluorescence yield for X-rays is excellent. As shown in Fig. 2, its counting efficiency decreases at energies below about 2 KeV because of the absorption of a Be window of 150 thick, and it also decreases above 100 KeV, because X-rays of such high energies go through the NaI(T1) crystal of 1.5 mm thick without appreciable absorption. A thin scintillator is able to avoid contaminating radiations such as cosmic ray particles.

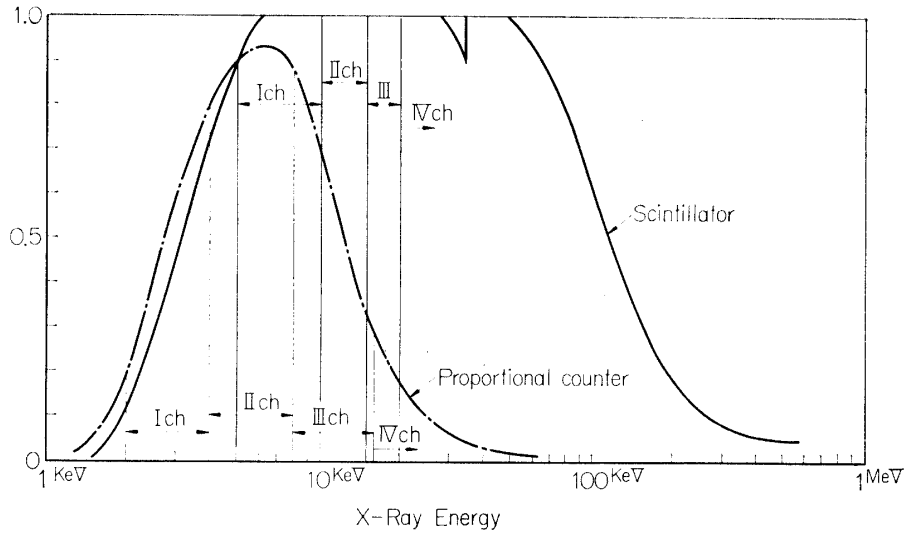

FIG. 2. Calculated counting efficiencies of a scintillator and a proportional counter for normal incidence of X-rays.

*) Manufactured by Horiba Co., Ltd., Kyoto, Japan.

2. Thermal noise of a photomultiplier

The fluorescent light produced in the scintillator was converted into photo-electrons, and the light excited thereby was amplified by a photomultiplier of RCA 6199. The thermal noise of the photomultiplier may mask signals of X-rays, if their energies are too low. Since the temperature at the top of the main stage, at which our counter was put, was known to be as high as 60°C, the thermal noise of the photomultiplier would become disturbing. However, the temperature inside a metalic case of a reflective surface was found to be kept as low as that before firing. Since our instrument was packed in an aluminium case, the temperature effect was believed to be harmless. Even if the temperature increases to 60°C, thermal noise was examined as negligible, so long as we are concerned with X-rays of energies greater than 5 KeV.

This is shown in Fig. 3, in which thermal noise is restricted to the pulse height range corresponding to the energies of an X-rays below 3 KeV.

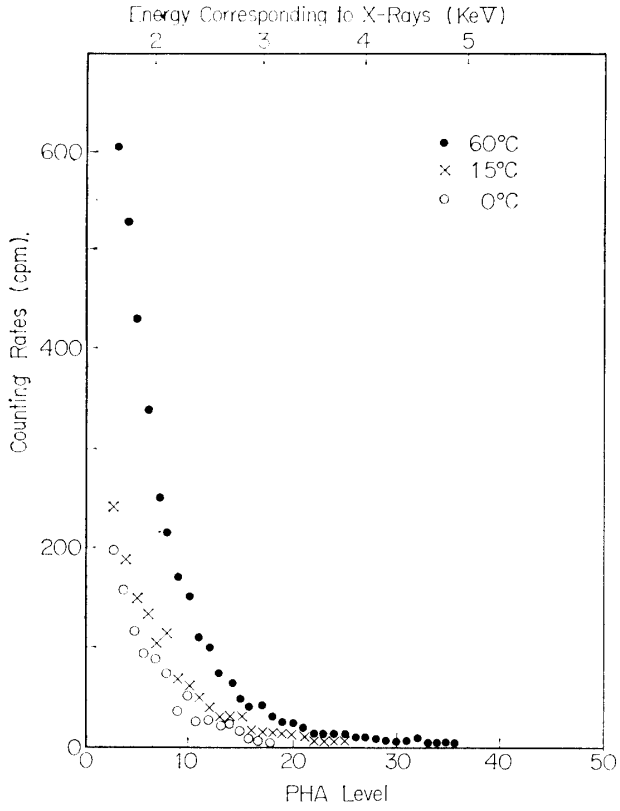

FIG. 3. Temperature dependence of thermal noise of a photomultiplier.

3. Energy resolution and linearity of a counter

In Fig. 4 we show the pulse height distributions obtained by the irradiation by X-rays from radioactive sources.

In Table III we list the average pulse heights and the energy resolutions obtained with these monochromatic X-rays.

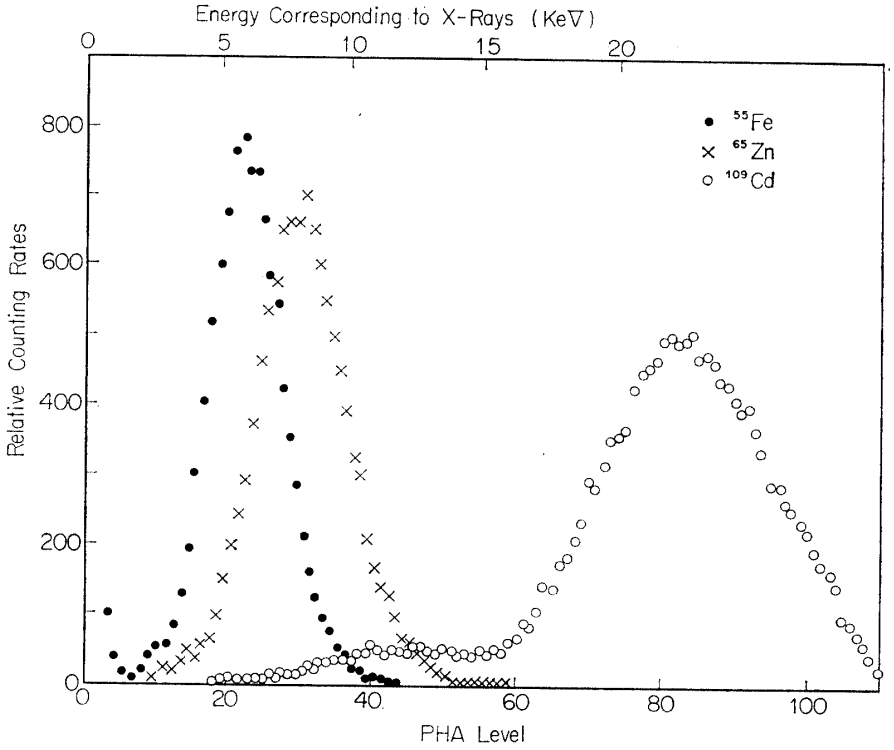

FIG. 4. Pulse height spectra of X-rays from ^{55}Fe, ^{65}Zn and ^{109}Cd detected with a scintillation counter.

The pulse height versus X-ray energy was found to be non-linear, possibly because the light collection efficiency, the fluorescence efficiency, and the spectral output of NaI(T1) may depend on energy.

Empirically the pulse heigh P, normalized at 5.9 KeV, is expressed as a function of X-ray energy k in KeV as

$$P=ak^2+bk \qquad \text{with } a=5.9\times10^{-3},\quad b=0.87. \tag{3}$$

This expression can reproduce the result given in Table III and is used to determine the energies of X-rays between 5 and 20 KeV. Considering this non-linearity, we must correct respective energy ranges in Table I to 5~9.7, 9.7~14.1, 14.1~18.2 and $\geq$18.2 KeV.

TABLE III. Average pulse height and energy resolution for X-ray detected with a scintillation counter.

X-ray energy	Pulse height/KeV	Energy resolution
5.89 KeV	1	58%
8.04	1.07	49
22.1	1.16	30

Incidentally, a similar non-linear behaviour was also found for NaI(T1) crystals by Engelkemeir [*13*].

The distribution of pulse heights is similar to Gaussian, and from our experiments

its half-width divided by the X-ray energy was obtained as

$$\eta=\frac{1.4}{\sqrt{k}}. \qquad (4)$$

This expression gives the energy resolution for X-rays in our counter. Since the fractional width increases with decreasing energy, a scintillation counter is not adequate to detect X-rays of energies below 5 KeV or so. The lower limit of the detectable energy is thus determined by the energy resolution as well as by thermal noise.

4. Angular resolution

The response of the counter depends on the direction of incidence of X-rays. The pulse height spectra of X-rays from ^{65}Zn are shown for various incident directions in Fig. 5. Although the counting efficiency depends greatly on the direction, the energy resolution was found to be essentially independent of the incident angle of X-rays. Nearly the same results were obtained for the pulse height distribution with other X-ray sources.

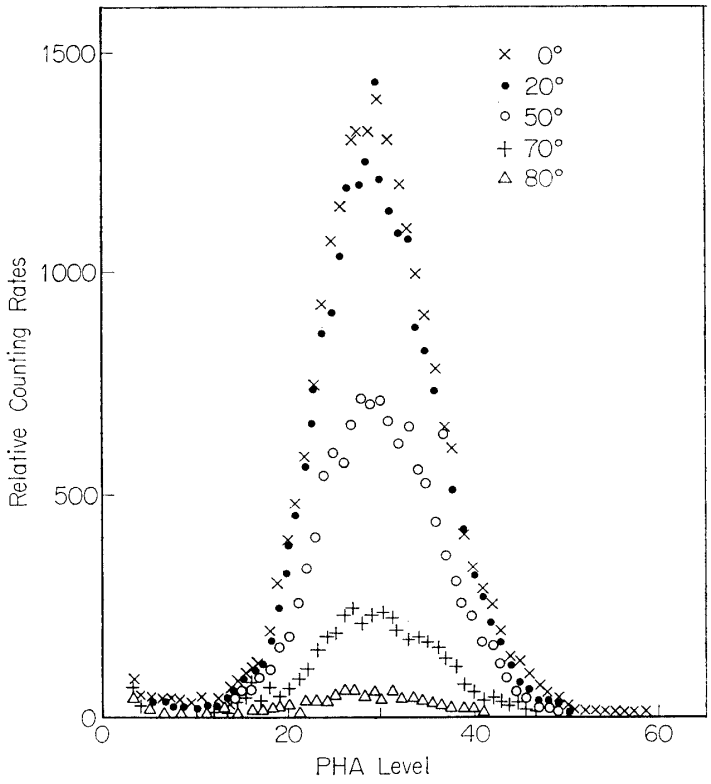

FIG. 5. Pulse height distributions of X-rays of 8.03 keV from directions of 0°, 20°, 50°, 70° and 80° detected with a scintillation counter.

On account of that the angular dependence is not sensitive to energy, it is meaningful to discuss the angular resolution of the counter without reference to energy. In Fig. 6 we show the angular resolution for X-rays of energies between 5 and 20 KeV. In analyzing the experimental data observed, three angular variables

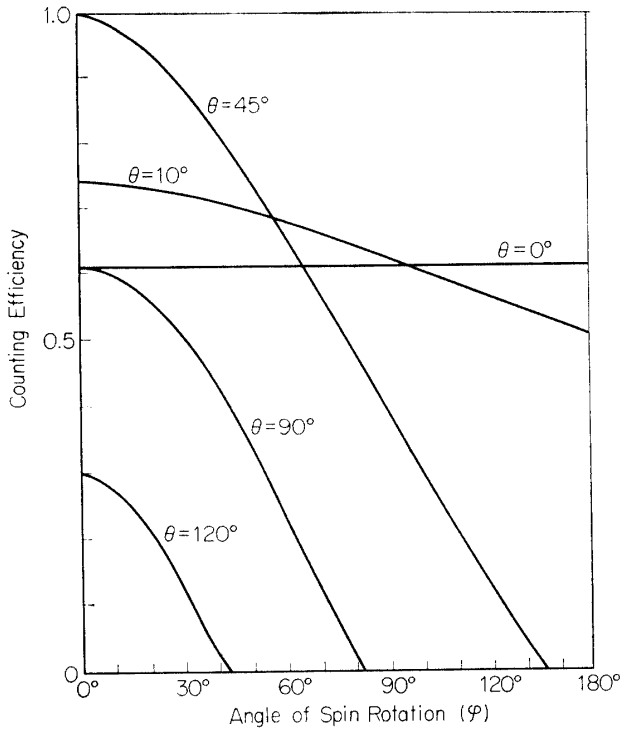

FIG. 6. Anglular response of a scintillation counter.

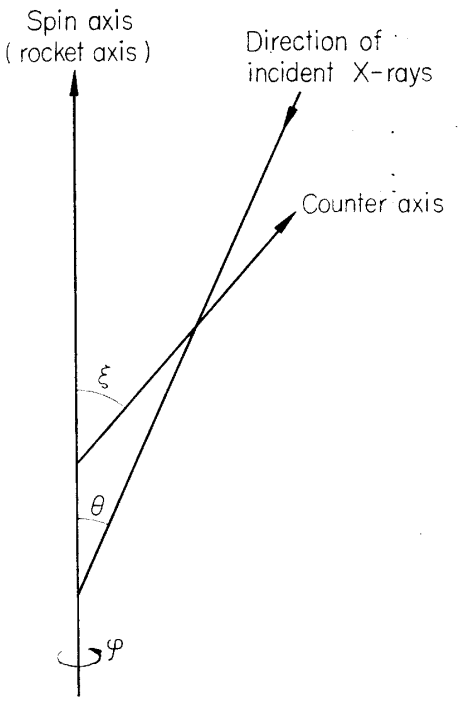

FIG. 7. Illustrative geometrical configuration for angular response.

have to be introduced as shown in Fig. 7. The angle between the spin axis and the direction of incident X-rays is denoted as θ, the angle between the rocket axis and the counter axis is fixed as $\xi=45°$, and the rotation angle with respect to the spin axis denoted as φ, where $\varphi=0°$ is defined as that the direction of X-rays lies in the plane containing the spin and counter axes.

5. Effects of contaminating radiations

Our counter is able to detect various kinds of radiation other than X-rays existing in the upper atmosphere. They include γ-rays, electrons, protons and heavy particles. We have, therefore, to eliminate effects of such contaminating radiation.

In Table IV we show the threshold energies of particles which could penetrate along normal line through the window without scattering and the minimum ionization loss which a relativistic particles produces when going vertically through a scintillator. It can be understood from this table that most of energetic charged particles from large pulses in a scintillation counter except for radiations of just near threshold energy. Pulse from our counter are discriminated to four regions corresponding to the approximate energy loss values of 5~10, 10~15, 15~20 and $\geq$20 KeV, called channels I, II, III and IV, where on account of the non-linearity in the pulse height-energy relation, these channels correspond respectively to the energy regions 5~9.7, 9.7~14.1, 14.1~18.2 and $\geq$18.2 KeV. Therefore pulses formed by charged particles would belong to the channel IV.

Effects of contaminating radiations were examined by using γ-rays from ^{137}Cs and β-rays from ^{147}Pm and ^{90}Sr. In each case the ratio of the counting rates of

TABLE IV. Threshold energy and minimum ionization loss in the scintillation counter (normal incidence).

	Threshold energy	Energy loss due to relativistic particles
Electron	150 KeV	990 KeV
Proton	4.1 MeV	1.1 MeV
α-particles	16 〃	4.5 〃

each channel to the total counting rates detected with a counter in shown in Table V. The detection efficiencies of 662 KeV γ-rays and β-rays from ^{147}Pm and ^{90}Sr are approximately estimated as 0.5, 0.1 and 0.8 respectively. It is noted from this result that the detection efficiencies in channel I~III are very small, and the contributions of such high energy radiations may be neglected, unless they are very strong.

TABLE V. Effects of γ-rays and β-rays in the scintillation counter.

Channel	Energy region	Ratio to total counting rates		
		γ-ray (662 KeV)	β-ray	
			max. 227 KeV	max. 542 KeV
I	5~9.7 KeV	0.014	0.15	0.014
II	9.7~14.1	0.0099	0.095	0.011
III	14.1~18.2	0.0089	0.088	0.0082
IV	≧18.2	0.96	0.68	0.93

Effects of ^{137}Cs γ-rays on channels I~III are considered as due to the Compton energy loss of γ-rays and the contamination of bremsstrahlung X-ray by β-rays from ^{137}Cs. Possible causes of contamination in channels I~III by β-rays are (1) bremsstrahlung X-rays excited in a Be window by β-rays, and (2) the energy loss of electrons with energies higher by several KeV than the threshold energy.

The contribution of (1) is important for electrons of energies from a several KeV to the threshold. An electron entering in a Be window loses its energy by ionization and bremsstrahlung. The bremsstrahlung efficiency of an electron of energy E in KeV is approximately expressed as $8\times10^{-6}E^{0.72}$ in consideration of the cross-section of bremsstrahlung and the range of the electron. If an observed counting rate of 1 count cm^{-2}sec^{-1} in channels I~III were attributed to electrons of several tens of KeV, the electron flux would have to be as strong as 10^4 cm^{-2}sec^{-1}.

If the residual energy of a charged particles after it passes through a Be window remains in the range from 5 to 20 KeV, the pulse formed by the particle would be obtained as the count of channels I~III. Since the ratio of such energy interval to the threshold energy concerned is 3×10^{-2} for an electron and 10^{-3} for a proton, flux intensities of charged particles would have to be stronger than those expected from counting rates in channel IV, in order that the charged particles give 1 count cm^{-2}sec^{-1} of channels I~III.

3.2. Proportional Counter

A proportional counter has the best energy resolution for X-rays among various photon counters in particular at low energies. In order to measure the energy spectrum down to 2 KeV, we used four proportional counters in K-9M-12 flight. Two of the counters formed one set and the other two formed another set facing against each other. Each counter had a side window as shown in Fig. 8. This counter system in Fig. 9 was installed, at the top of the main stage of the rocket, K-9M-12. This arrangement of the counters was adopted for increasing the detection area and eliminating high energy charged particles due to the anticoincidence method. This subsection is devoted for discussions of various properties of the proportional counter.

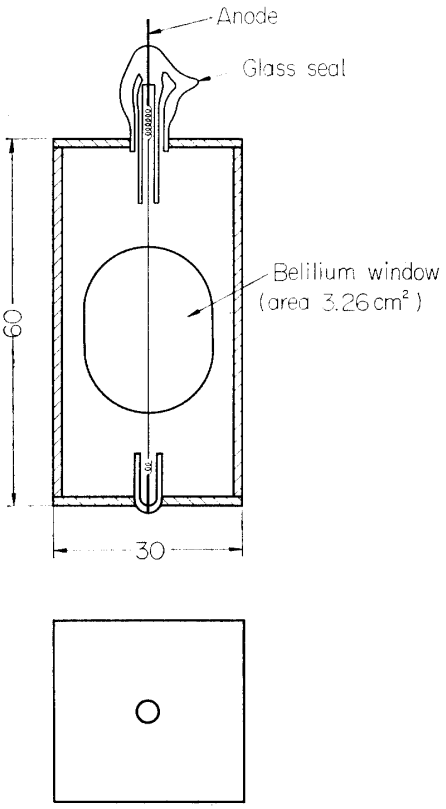

Fig. 8. Two side views of a proportional counter (mm unit).

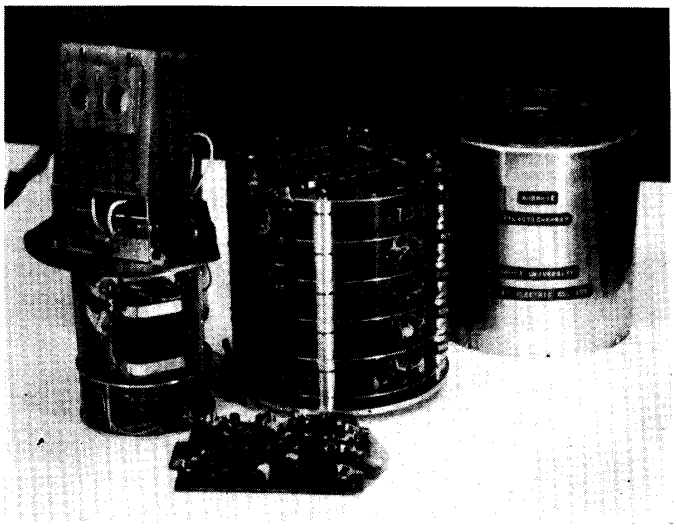

Fig. 9. The X-ray instrument with proportional counters borne on the rocket, K-9M-12. On the left in this photo four proportional counters packed and high tension supplies, in the center the electronic system and on the right the case of electronic system are shown.

1. Counting efficiency

Fig. 2 shows the counting efficiency for X-rays of normal incidence. In the case of oblique incidence the counting efficiency is slightly dissimilar to that of normal incidence. This effect is taken into account in calculating the angular resolution shown in subsection 3.

2. Energy resolution and its age effect

Our seal off proportional counter showed an age effect, according to which the pulse height and consequently the energy resolution decrease with the lapse of time.

The decline of an energy resolution, η, was as follows; we were able to obtain $\eta \simeq 0.5/\sqrt{k}$ just after gas was filled, but the energy resolution became $\eta \simeq 0.8/\sqrt{k}$ for those counters which were left for checking several months after the flight. In order to get rid of the age effect, the pulse height-energy relation was calibrated just before the rocket flight.

The age effect of gas seal off counters seems to becaused by (1) a very slow leak of air gas through a thin window, and (2) the contamination of harmful gas due to the decomposition of quenching gases. We can, however, avoid the case (1) if we carefully select a window film without pinholes.

3. Angular response

The pulse height due to an X-ray depends considerably on the incident angle, for our proportional counter has no guard ring to get rid of the end effect; if photo-electrons are produced towards an end of the counter, the pulse height produced thereby in smaller than that due to an X-ray absorbed in the central region. Although a window is located in the central part, X-rays of small angles with the anode line of a counter may be absorbed in the end region and produce relatively small pulse heights. In Fig. 10 are shown the pulse heights of experimental points

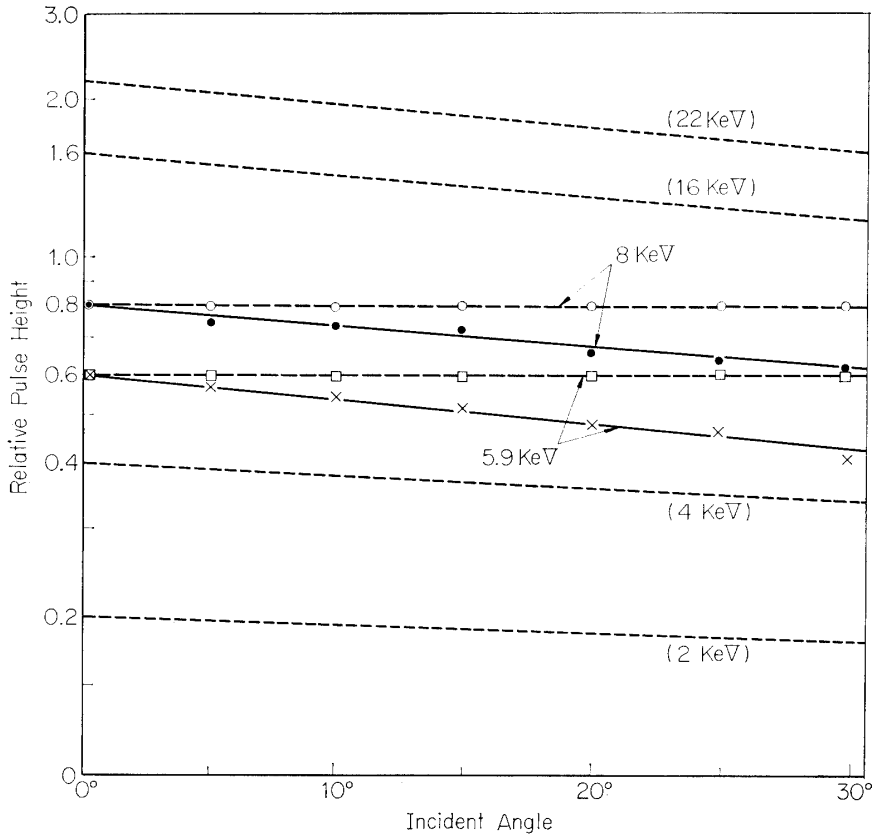

FIG. 10. Angular response of pulse heights. Solid lines and dotted lines denote those for X-rays of incident angles perpendicular to the anode line of a counter and dashed lines those for X-rays of incident angles on the plane perpendicular to the anode lines. Marks, ●, ○, × and □ denote experimental values.

against the incident angle of 5.9 KeV X-rays and 8.04 KeV X-rays. 22.1 KeV X-rays from ^{109}Cd were not used because of contaminating radiations of ^{109}Cd. For other energies the incident angle dependences of pulse heights are extrapolated from this experimental result as shown by dotted lines. It is also noted from dashed lines in this figure that the pulse height versus incident angle is constant if the direction of an incident X-ray lies in the plane perpendicular to the anode line of a counter.

These angular dependences served to obtain the energies of X-rays from a given source from the pulse heights observed by knowing the aspect of our counters by referring to the data of a geomagnetic aspectmeter.

The angular response versus the spin rotation of a rocket was calculated for various energies of X-rays, on account of the geometrical configuration like as in Fig. 7, but with $\xi=75°$ and $\xi=105°$. Some examples of the efficiency versus angle are shown in Fig. 11. These results are taken into account in the analysis of our experimental data.

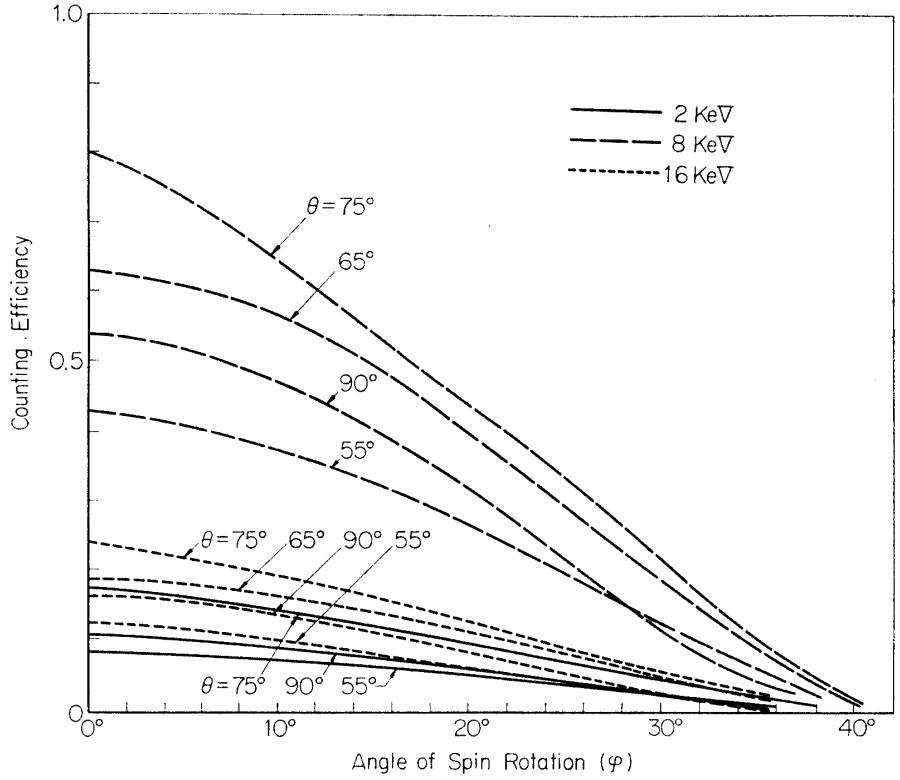

FIG. 11. Angular responses calculated for X-rays of 2, 8 and 16 KeV for a proportional counter in the case of $\xi=75°$.

4. Effects of contaminating radiations

Fig. 12 shows the pulse height spectra of γ-rays and β-rays detected with our proportional counter. One might aware, looking at this figure, that γ-rays and β-rays would become a strong background in channels I~III, but they are not serious because of their low counting efficiency as discussed in what follow.

γ-rays form contaminating pulses due mainly to the Compton effect. This effect,

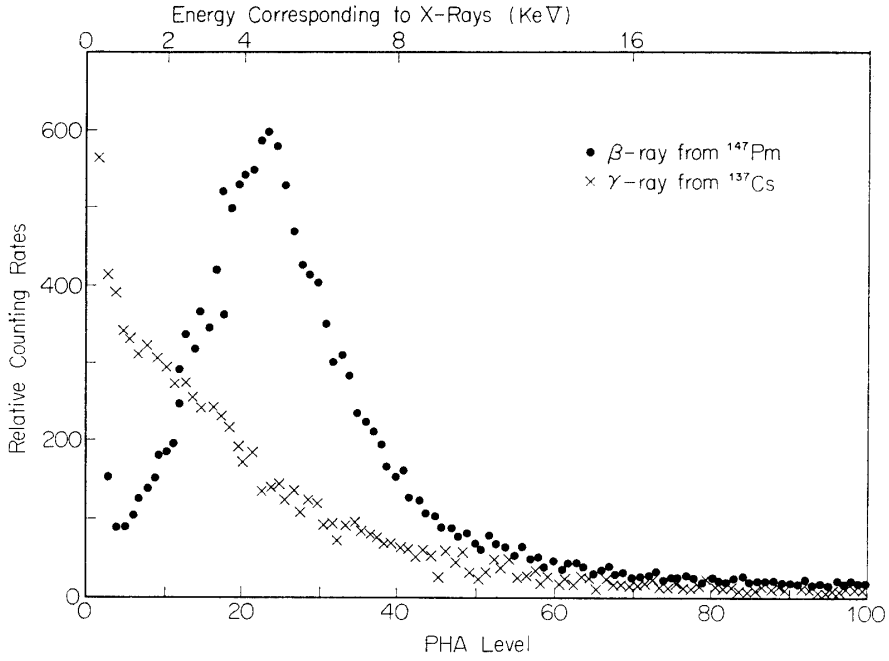

FIG. 12. Spectral distributions of γ- and β-rays detected with a proportional counter.

however, would be negligible for the conversion efficiency of γ-rays with energies between 1 MeV and 16 KeV owing to a small Compton cross section; the counting efficiency due to the Compton effect is estimated to be as small as 10^{-5} in gases of our proportional counter. Therefore, the counting rates in 2~16 KeV due to γ-rays are far smaller than those of galactic X-rays unless the flux intensity of γ-rays were as intensive as 10^5 cm^{-2}sec^{-1}sr^{-1}.

Effects of charged particles may be seen from Table VI. General expressions for energy losses of non-relativistic particles in our counter are

$$-\frac{dE}{dx}=\frac{72}{E}\ln\frac{E}{0.64}\quad \text{KeV/cm}, \tag{5}$$

for an electron of energy E in KeV, and

$$-\frac{dE}{dx}=\frac{1.3\times 10^2}{E}\ln\frac{E}{0.34}\quad \text{KeV/cm}, \tag{6}$$

for a proton energy E in MeV.

TABLE VI. Properties of charged particles in a proportional counter.

Charged particles	Threshold energy in normal incidence	Energy loss due to relativistic particles	Energy corresponding to the range of gas thickness
electron	120 KeV	2.5 KeV/cm	67 KeV
proton	2.3 MeV	2.9 〃	1.3 MeV
α-particles	9.4	12	5.1 〃

In order to illustrate the effects of electrons and protons, we consider only charged particles of normal incidence; in the case of oblique incidence results can be obtained with suitable corrections.

Electrons of energies below 200 KeV have the same effects as described in 3.1. 5; they lose energies higher than 20 KeV in Xe gas and have no effect in channels I~III. Bremsstrahlung X-rays emitted in the Be window are also negligible because of the same conversion efficiency as described in that section. Electrons above 200 KeV lose several KeV in a counter, but in this case they could be rejected with the aid of the anticoicidence, because they have chances to penetrate two counters. This circumstance is the same for protons of energies greater than 10 MeV. A troublesome problem for high energy particles lies in the fact that a particle loses its energy only in one counter. This probability is estimated as about 10^{-3} on account of the geometrical configuration of counters.

As a summary, radiations detected in channel IV are X-rays, electrons of energies between 100 and 200 KeV, protons of 2~10 MeV and heavy particles. Radiations detected from channels I to III are X-rays, electrons above 200 KeV and protons above 10 MeV. Relativistic particles contribute mainly to channel II.

In the upper atmosphere radiations other than X-rays are expected to be so weak that our purpose of the observation of galactic X-rays would be satisfied.

3.3. GM Counter

A GM counter has been a simple instrument to detect X-rays since long ago. A GM counter by itself cannot discrimmate the energies of incident radiations, because a pulse from this counter can be formed by only one ion pair produced in its gas. A pulse height distribution was measured so narrow that the ratio of a full width at half maximum to the pulse height at maximum was about 10^{-3}. We can, however, make a GM counter sensitive mainly to some radiation designing a size and a gas pressure fitted to our purpose.

1. Counting efficiency

We made three types of GM counters sensitive mainly to X-rays as shown in Table 1. The structure of the GM counter used for the observation of galactic X-rays is an end-window type as shown in Fig. 13. Fig. 14 shows the arrangement of 23 GM counters to be borne on the rocket, K-9M-15.

In Fig. 15 we show the counting efficiency calculated for normal incident X-rays. This is consistent with the experimental result obtained with K X-rays of ^{55}Fe; the plateau curves of respective counters are shown in Fig. 16.

2. Angular response.

Each counter was equipped with a cylindrical collimator of $25\phi \times 30$ mm made of a plastic material. The collimator limited the field of view to the full width at half maximum of about 24° in the direction of rotation of a rocket, but the actual half maximum angle depends on the energy or wave-length of incident X-rays. The

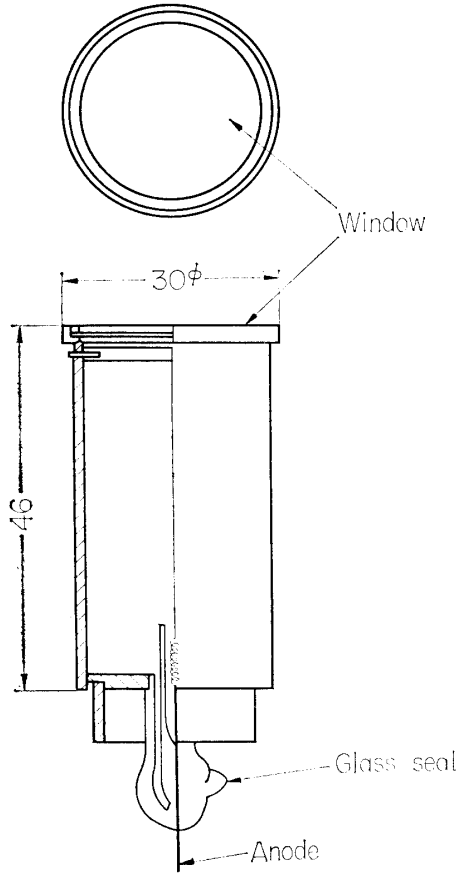

FIG. 13. Two side views of a GM counter (mm unit).

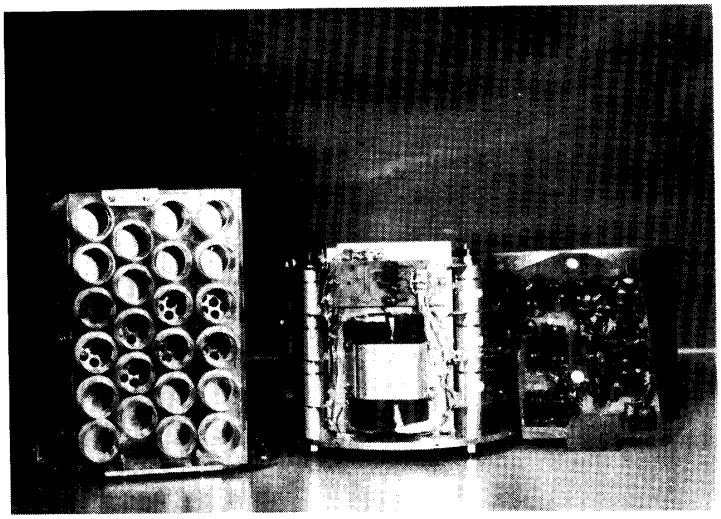

FIG. 14. The X-ray instrument with GM counter borne on the rocket, K-9M-15. On the left in this photo twenty-three GM counters are shown.

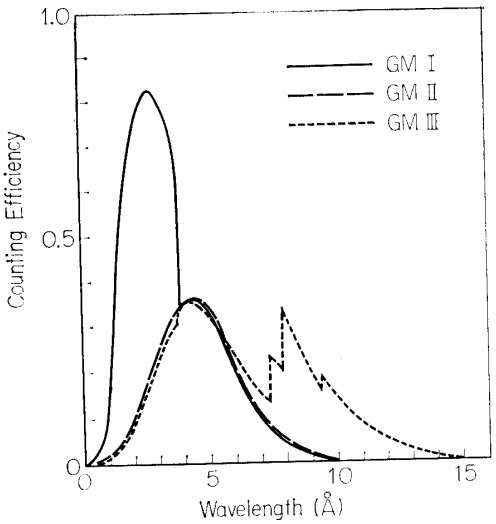

FIG. 15. Counting efficiencies of GM counters for normal incidence of X-rays.

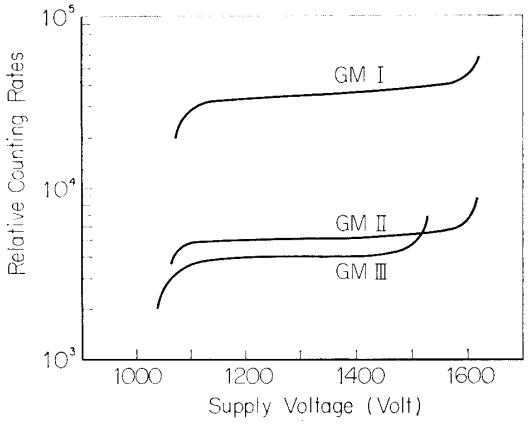

FIG. 16. Plateu curves of GM counters. Experimental results due to X-rays radiated from ^{55}Fe.

angular response versus the spin rotation of a rocket calculated for various wavelengths of incident X-rays are shown in Fig. 17. In our calculation three angular

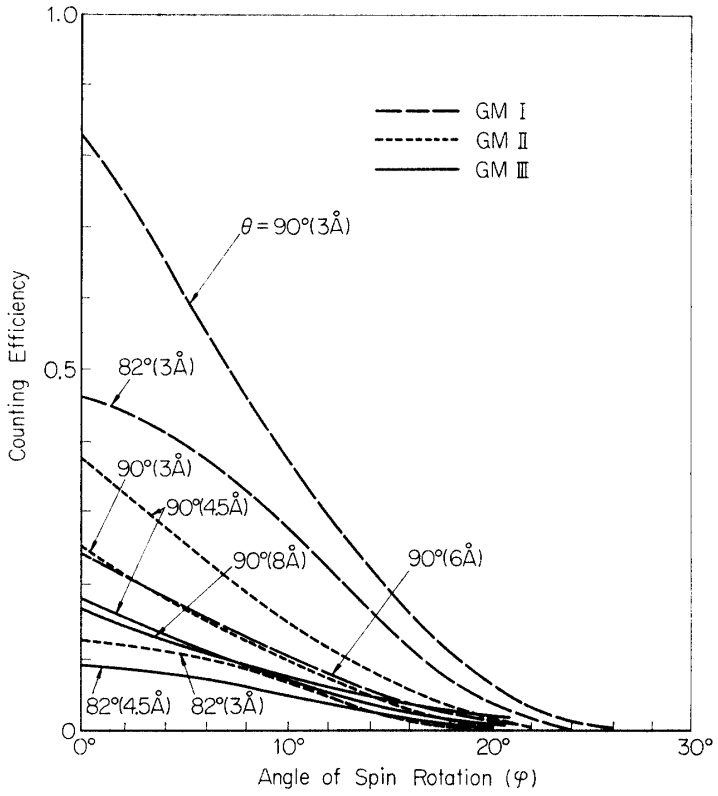

FIG. 17. Examples of angular responses of X-rays calculated for GM counters.

variables are again introduced as shown in Fig. 7 in 3.1.4; in this case the angle between the rocket axis and the counter axis was fixed as $\xi=90°$.

3. Effects of contaminating radiations

Even a hard X-ray with a fairly low efficiency would produce photoelectrons at the inner wall of a counter and form a pulse. This efficiency is estimated as about 10^{-2} for 22 KeV X-rays and decreases gradually as energy increase. γ-rays also form pulses by Compton scattering in a counter gas. The Compton scattering probability is of the order of 3×10^{-3} in Ar-gas and 10^{-4} in Ne-gas. The photon component other than X-rays concerned, therefore, has only a negligible contribution as contaminating radiations.

Any charged particles entering a counter would form pulses with an efficiency of about 100 per cent. Therefore most of charged particles higher than threshold energies listed in Table VII are sensitive to our GM counters. Relativistic charged particles would penetrate two or more counters with some probability; hence they would be rejected with an anti-coincidence circuit. The rejective probability is estimated as about 20%. We would be able to obtain an approximate upper limit of intensities of charged particles higher than the threshold energies from the isotropic component observed. Then we can subtract counting rates of charged particles from observed ones, but it would be fairly difficult to obtain the absolute intensities of X-rays.

TABLE VII. Threshold energies of charged particles for GM counters.

Particles	GM-I, II	GM-III
electron	120 KeV	22 KeV
proton	2.3 MeV	300 〃
α-particles	9.4 〃	1.2 MeV

4. ELECTRONIC SYSTEM

All electronic circuits were transistarized, and were ordinary, as far as their working principles were concerned. Improvement was, however, made for compactness and stable performance against shock, vibration, vacuum, and high temperature as a rocket-borne instrument.

Fig. 18 shows the block diagrams of three counter systems. Sorting pulses from a scintillation counter and a proportional counter with a pulse height analyzer,

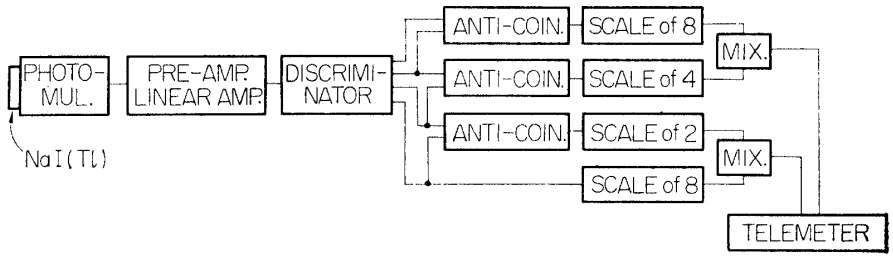

a Scintillation counter system.

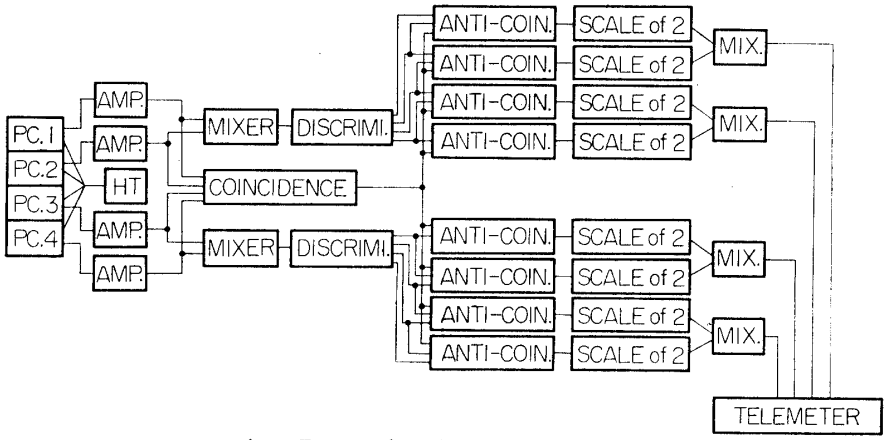

(b) Proportional counter system.

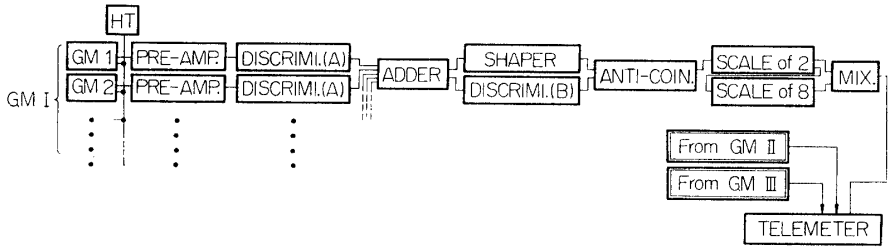

(c) GM counter system.

FIG. 18. Block diagram of counter systems.

digitazed counting rates of X-rays from respective energy ranges concerned are obtained, for a pulse height from these counters approximately linear to the energy detected; on the other hand a pulse height from a GM counter in nearly constant. However since our GM counters by themselves are sensitive mainly to X-rays in these wavelength ranges, a digitazed output from each type of GM counters would give the X-ray intensity of a wavelength range concerned unless contaminating radiations are too strong. A relativistic charged particle is rejected with an anti-coincidence circuit when it penetrates two or more counters.

Ni-Cd batteries were used as the primary power supply. Since the variation of the primary voltage of this battery was about 20% for the current of 100 mamp. for one hour. We designed each circuit element to work stably under this circumstance. The total power consumption was about 1.5, 4.0 and 2.5 W respectively for a scintillation counter system, a proportional counter system and a GM counter system.

Most of circuits described in this section were tested by balloon-borne experiments and the whole systems were tested against severe environmental conditions such as shock, vibration and high temperature. Results of these tests showed sufficient stabilities of the whole systems.

1. High voltage supply

The circuit of the high voltage supply for a photomultiplier, a proportional counter or a GM counter was slightly improved in comparison with described in our previous paper [*14*]. A high voltage was stepped up from a primary voltage of 12 volt by means of a DC to DC converter. Under the temperature from $-10°C$ to $60°C$ and the input voltage from 15 V to 10 V, its output voltage was found to vary within about 0.3%.

This part was packed by beas-wax to prevent discharge under the low atmospheric pressure. This package also surved for thermal shielding as well as for a shock and vibration absorber.

2. Amplifier

We adjusted the input impedance of a pre-amplifier so that the decay constant of an exponential pulse was 10 μsec. The amplifiers for a scintillation and proportional counters had the maximum gain of about 25 db and had the best linearity for the exponential pulse of a 10 μsec pulse. The gain was found to change less than 0.3% under the temperature from $0°C$ to $60°C$ and the input voltage from 10 to 14 V.

3. Puse height discriminator

A modified schmitt circuit was used to discriminate pulse heights. We used a Zener diode ls551 to supply a constant DC voltage to each transistor base bias. The stability of the discriminator, therefore, was better than 0.1% for the temperature variation from $0°C$ to $60°C$ and also for the variation of the primary voltage from 10 V to 15 V. Since a pulse was divided suitably at the emitter-follower of

the last stage of an amplifier by means of resistors, discrimination levels were set only to 0.5 volts for the scintillation counter system and only to 0.2 volts for the proportional counter system. The discrimination level for a pulse from a GM counter was adjusted so as to allow almost all pulses to pass through.

4. Performance of an anti-coincidence

Two adjacent discriminators were connected to the anti-coincidence circuit which was able to pass pulses from only one discriminator but to cut off others. The dead time of this circuit was adjusted to 20 μsec at most. This device also performed stably under variations of the temperature and the primary voltage.

5. Flip-Flop unit

A packed unit manufactured was used as a flip-flop circuit in order to scale down the counting rate whose response frequency was less than 15 kc/s, since our counting rates were expected as $\lesssim 1$ kc/s, and the rise time and the decay time were $\lesssim 2\mu$ sec and $\lesssim 5\mu$ sec respectively. Stability tests showed its satisfactory performance under our rocket-borne condition.

6. Performance of an adder and a shaper-discriminator (B)

Pulses from one GM counter are added to those from others by an adder circuit. If two or more counters work simultaneously, an output pulse from the adder is higher and is able to pass through both pulse shaper and discriminator circuits, whereas, if only one counter works, an output pulse from the adder can pass through only a pulse shaper circuit. This means that in the former case no output pulse comes out of an anti-coincidence circuit, but in the latter case a pulse comes out.

7. Mode of outputs of information

Fig. 19 shows the mode of the input to the telemeter which transmit information by the FM-FM method of main carrier wave of 295 Mc/s. Variations of normal to a base line mean the information of radiations detected. Two pieces of information

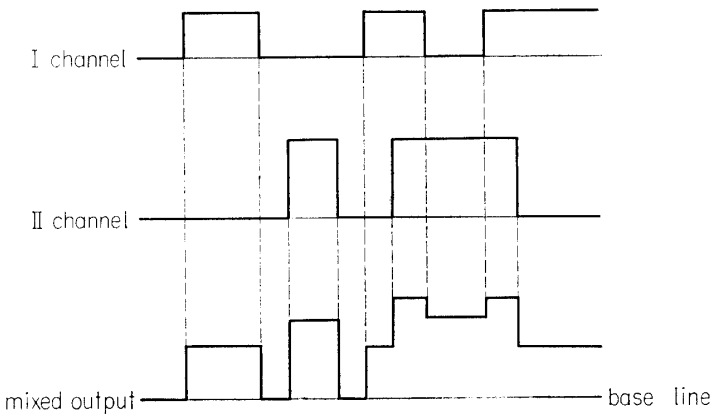

FIG. 19. Output mode of X-ray records.

were often mixed but were discriminated by different pulse heights. One can obtain counting rates in each channel from this digitazed output.

5. Data Analysis

Raw data observed include the information of radiations of charged particles and atmospheric X-rays in addition to galactic X-rays.

Since the attitude of a counter varies according to the spin and precession of a rocket, we accumulate the counting rates at a direction fixed in space by reference to the aspect of the counter. This procedure is of great help in distinguish three types of radiations from each other. The atmospheric X-rays are expected as the strongest in the horizontal direction, and their contribution can be obtained from the directional dependence of the counting rate. Charged particles are more or less isotropic, and may increase with altitude if they are related to radiation belts. X-ray sources can be identified with peaks of the counting rate at fixed spatial directions. In order to obtain the spectral shapes of galactic X-rays, the correction for the angular dependence of efficiency is necessary. All of those mentioned above can be achieved by knowing the counting rates at given spatial directions.

5.1. A Deduction Method of Aspects of a Detector

In order to calculate the aspect of a counter we refer to the geometrical configuration as shown in Fig. 20, where ζ is the angle between the precession axis and the spin or rocket axis, ξ the angle between the rocket axis and the counter axis, Φ and Θ mean the right assension and the declination of the direction of the precession axis.

A spatial direction of a counter is represented by the right assension α and the declination δ, and they are related to the local direction represented by ζ, ξ, Φ, Θ, φ and ψ as

$$\left.\begin{aligned}\cos\delta = {} & \cos\Theta\cos\Phi(\cos\zeta\cos\psi\cos\varphi\sin\xi - \sin\psi\sin\varphi\sin\xi \\ & + \sin\zeta\cos\psi\cos\xi) - \sin\Phi(\cos\zeta\sin\psi\cos\varphi\sin\xi \\ & + \cos\psi\sin\varphi\sin\xi + \sin\zeta\sin\varphi\cos\xi) + \sin\Theta\cos\Phi(\cos\zeta\cos\xi \\ & - \sin\zeta\cos\varphi\sin\xi),\end{aligned}\right\} \quad (7a)$$

$$\left.\begin{aligned}\sin\delta\sin\alpha = {} & \cos\Theta\sin\Phi(\cos\zeta\cos\psi\cos\varphi\sin\xi - \sin\psi\sin\varphi\sin\xi \\ & + \sin\zeta\cos\psi\cos\xi) + \cos\Phi(\cos\zeta\sin\psi\cos\varphi\sin\xi \\ & + \cos\psi\sin\varphi\sin\xi + \sin\zeta\sin\psi\cos\xi) \\ & + \sin\Theta\sin\Phi(\cos\zeta\cos\xi - \sin\zeta\cos\varphi\sin\xi),\end{aligned}\right\} \quad (7b)$$

$$\left.\begin{aligned}\sin\delta\cos\alpha = {} & -\sin\Theta(\cos\zeta\cos\psi\cos\varphi\sin\xi - \sin\psi\sin\varphi\sin\xi \\ & + \sin\zeta\cos\psi\cos\xi) + \cos\Theta(\cos\zeta\cos\xi \\ & - \sin\zeta\cos\varphi\sin\xi),\end{aligned}\right\} \quad (7c)$$

where, introducing ω_s and ω_p as angular velocities of spin and procession respectively, φ and ψ are given as

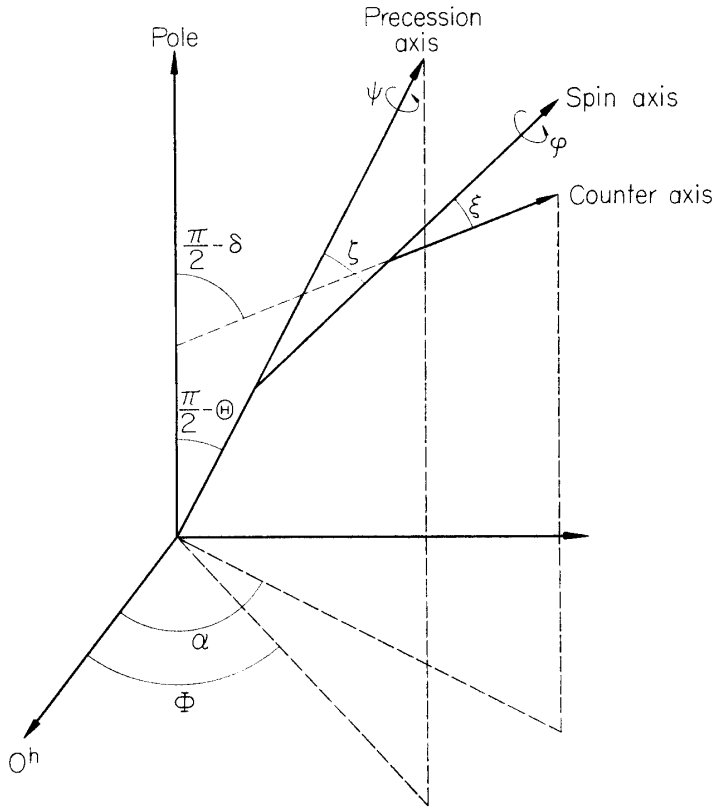

FIG. 20. Illustrative geometrical configuration to calculate the aspect of a counter on a rocket.

$$\left.\begin{aligned}\varphi&=\omega_s(t+t_0)\,,\\ \psi&=\omega_p(t+t_0)\,.\end{aligned}\right\} \tag{8}$$

In order to calculated expression (7) numerically it is necessary to find the aspect of a counter at a time, t_0, as an initial condition with the aid of the aspectmeter. If a rocket flies steadily after to the aspect of a counter can be obtained for arbitrary time from (7). The aspectmeter borne on a rocket is a geomagnetic aspectmeter*) with which an aspect is determined is accuracy of a few degree. Our sounding rockets may be expected to fly steadily after the nose cone is opened.

5.2. A DEDUCTION METHOD OF SPECTRAL SHAPES OF GALACTIC X-RAYS

1. Data from a scintillation counter and a proportional counter.

A pulse height distribution of monochromatic X-rays detected with a scintillation or a proportional counter is approximately Gaussian. The Gaussian distribution function is shown as

$$f(k, k_0)dk=f_0 e^{-\frac{(k-k_0)^2}{2\sigma^2}}dk\,, \tag{10}$$

where f_0 is the normalization factor $\int_0^\infty f(k, k_0)dk=1$.

*) Designed by Professor Y. Kato and his group of Tohoku University.

Introducing the half width, Δ to be related with the energy resolution, $\eta=\Delta/k_0$, the standard deviation, σ, is expressed as

$$\sigma=\frac{\Delta}{2\sqrt{2\ln 2}}.$$

We can obtain spectral shapes of X-rays detected making use of the expression (10). If corrected counting rates per unit time of i-channel (energy range $k=k_1\sim k_2$) is detected as n_i from a certain direction the following relation is obtained;

$$\int_{k_1}^{k_2}dk\int_0^{\infty}dk_0 j(k_0)G(k_0)\varepsilon(k_0)f_0\,e^{-(k-k_0)^2/2\sigma^2}=n_i, \tag{11}$$

where $G(k_0)$ in the geometrical factor of a counter for the energy k_0 and $j(k_0)dk_0$ is the differential spectrum of X-rays. $j(k_0)dk_0$ is assumed as two cases, that is,

1) Power spectrum

$$j_1(k_0)dk_0=j_{01}k_0^{-\gamma}dk_0. \tag{12}$$

2) Exponential spectrum

$$j_2(k_0)dk_0=j_{02}e^{-k_0/T}dk_0/k_0. \tag{13}$$

It is our purpose that γ and T are calculated from the equation (11). Since we can not solve the integral equation (11) analytically, a computor is used. As we discussed the geometrical factor $G(k_0)$ and the efficiency $\varepsilon(k_0)$ in 3, they depend of the flight condition of a rocket as well as the position of a counter on the rocket.

2. Data from a GM counter

A pulse height distribution from a GM counter is monochromatic as discussed in 3.3. Therefore if X-rays lose their energies in a GM counter, almost all pulses would be sent to the input of a telemeter.

If the geometrical factor of counters for a certain rocket flight is $G(\lambda)$ for the wavelength λ, one can obtain the similar relation as the expression (11);

$$\int_0^{\infty}j(\lambda)\varepsilon_i(\lambda)G_i(\lambda)d\lambda=n_i, \tag{14}$$

where n_i is corrected counting rates per unit time observed with i-counter, $\varepsilon(\lambda)$ its efficiency and $j(\lambda)d\lambda$ is the flux intensity of X-rays assumed for the wavelength between λ and $\lambda+d\lambda$.

6. Rocket-Borne Instruments and Results of Observations

Three types of X-ray instruments which were described in this paper were borne on Japanese sounding rockets, or which other instruments were also borne together; a two-stage rocket and a three-stage rocket named Kappa-9M and Lambda-3 respectively. Weight, size and payload of these rockets are listed in Table VIII.

These rockets were launched from the Kagoshima Space Center at Uchinoura in charge of Institute of Space and Aeronautical Science, University of Tokyo. Three types of X-ray instruments performed rather well during rocket flights, but a half

of four proportional counters were broken down just before the rocket flight. General discription of those flights in given in Table IX.

TABLE VIII. Specification of sounding rockets.

Rocket	Total length	Diameter of main stage	Total weight	Payload of total physical instruments	Payload of the X-ray instrument	Observation item*)
L-3-3	19.11 m	420 mm	7047.8 kg	97.9 kg	3.0 kg	CR, GA, GX ID, PR, RN
K-9M-12	11.11	250	1432.9	35.5	7.8	GA, GX, ZL
K-9M-15	11.19	250	1439.9	38.4	8.3	AG, GA, GX ID, RN

*) *Abbriviation* AG: air glow, CR: cosmic rays, GA: geomagnetic aspectmeter, GX: galactic X-rays, ID: ion density, PR: propagation of electromagnetic wave, RN: radio noise, ZL: zodiacal light.

TABLE IX. General discription of rocket flights.

Code	Type of rocket	Time of launching	Maximum altitude	Nose cone opening altitude
GX-1	L-3-3	Mar. 18, 1965, 1907 JST	1090 km	155 km
GX-2	K-9M-12	Jul. 26, 1965, 2101 JST	350 km	73 km
GX-3	K-9M-15	Mar. 20, 1966, 2150 JST	300 km	60 km

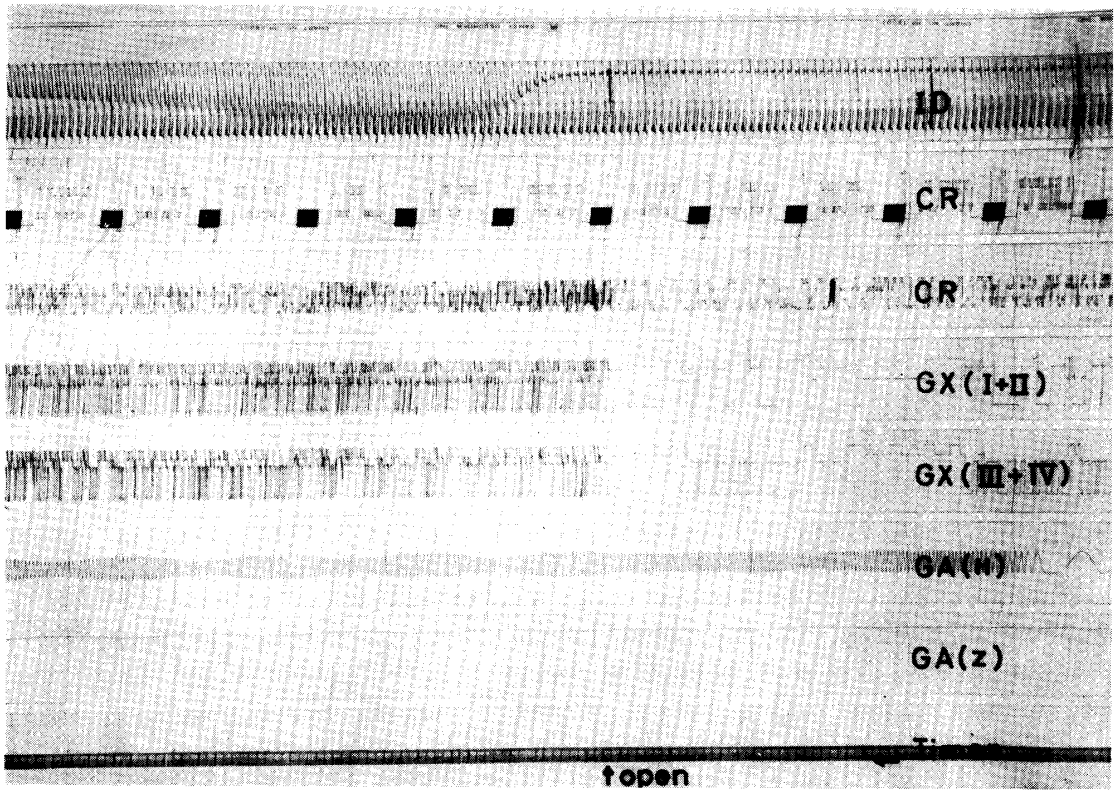

FIG. 21. A part of records of output from a receiver for the telemeters in L-3-3. Notice that the counting rates suddenly increased when the nose cone was opened.

Here we describe some properties of raw data. Fig. 21 shows a part of records of output from a receives of the telemeter of L-3-3. It is noticed from this figure that X-rays are detected as soon as nose cone opened. As listed in Table I response frequencies of telemeter were 45 c/s and 35 c/s. Scince mixed counting rates of channels III and IV were unexpectedly higher than the response frequency, some of them would have been missed. Moreover it is rather difficult to reject contaminating radiations such as charged particles and albedo X-rays completely only from results of GX-1. These detailed corrections will be made with a statistical treatment in reference to the observations which were carried out with a rocket, L-3H-1, as well as, GX-2 and GX-3.

In Fig. 22 counting rates obtained in GX-1 from the north direction and south direction are shown according to the altitude. It is seen that the counting rates increase with altitude in all but channel III. The increase is steeper in the north direction than in the south one again in all but channel III. The counting rate in channel III is as due to a low response frequency of the telemeter channel, and therefore, the missing probability of counts in channel III increases with the counting rate in channel IV. The correction for this effect indicates that the counting rate in channel III must have behaved in the same way in other channel. In the intensities in the north and the south directions being extrapolated to low altitude,

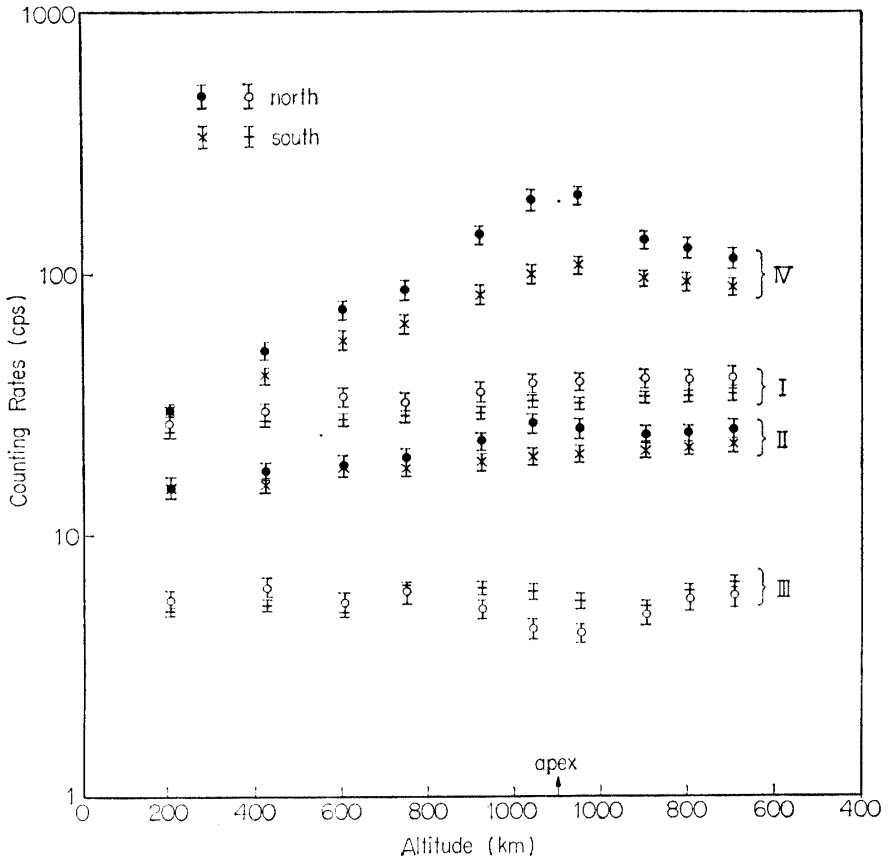

FIG. 22. Counting rates obtained in GX-1 from the north direction and the south direction.

their differences vanish at an altitude in all channels. The intensities at this point are defined as the isotropic intensities which may be regarded as due to galactic X-rays.

Fig. 23 shows the counting rates with respect the spin angle. Peaks in the figure are identified with X-ray sources of Sco X-1 and Cyg X-1. The heights of these peaks depend on the precession angle, as shown in Fig. 23(a) and (b). We can deduce the intensities of X-rays from Sco X-1 and Cyg X-1 by subtructing the isotropic intensity.

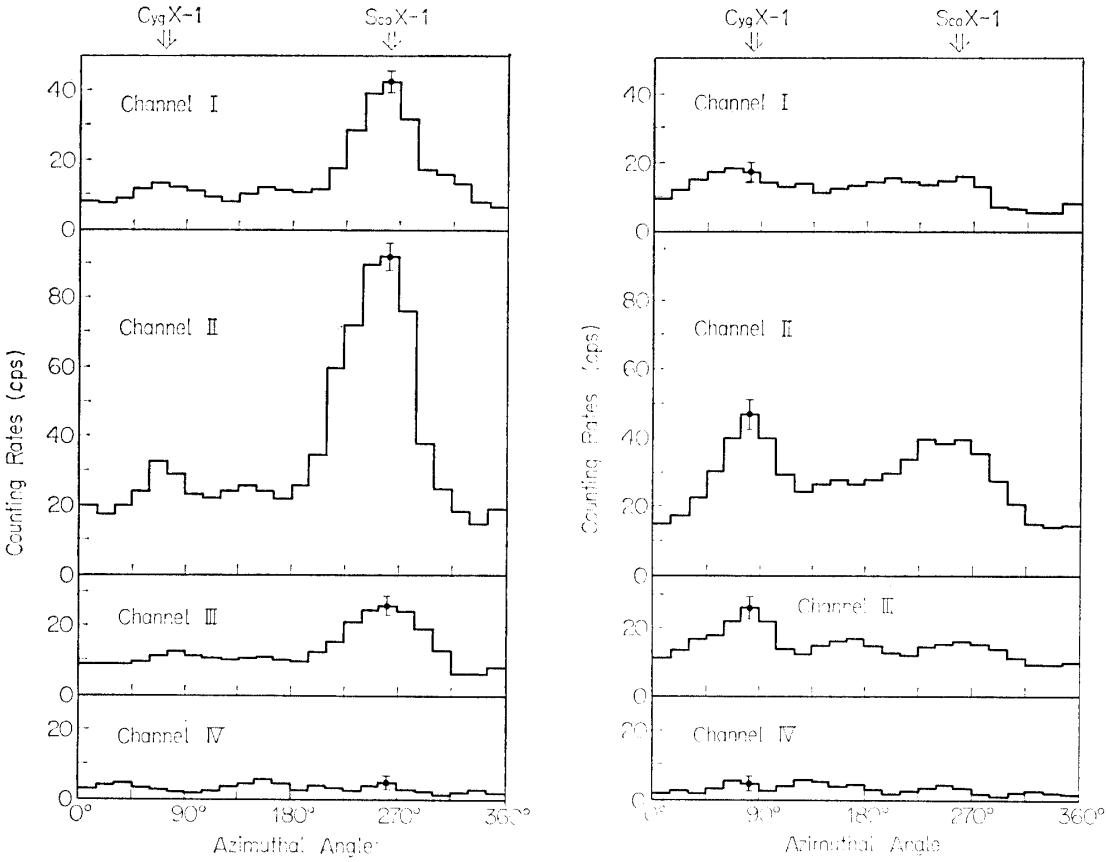

(a) The precession angle was in favour of detecting Sco X-1 rather than Cyg X-1.

(b) X-ray counters scanned the nearest direction of Cyg X-1.

FIG. 23. Counting rates with respect to the rocket spin angle in GX-2.

The GX-3 experiment gave the X-ray spectrum in a low energy region from the Crab nebula and the isotropic X-ray intensity of the wavelength range between 1.5 and 3.9 Å. The counting rate versus spin angle in Fig. 24 showed a peak identified as due to the Crab nebula. We can deduce the best fits of an exponential spectrum and a power spectrum using the method of 5.2.

Preliminary results of energy spectra of isotropic X-rays due to galactic and atmospheric origins are shown in Fig. 25. The former can be smoothly connected with intensities obtained by other groups. The L-3H-1 experiment in this figure was attempted in order to distinguish between X-rays from space and of the atmospheric origin. Two scintillation counters similar to that of the L-3-3 experiment

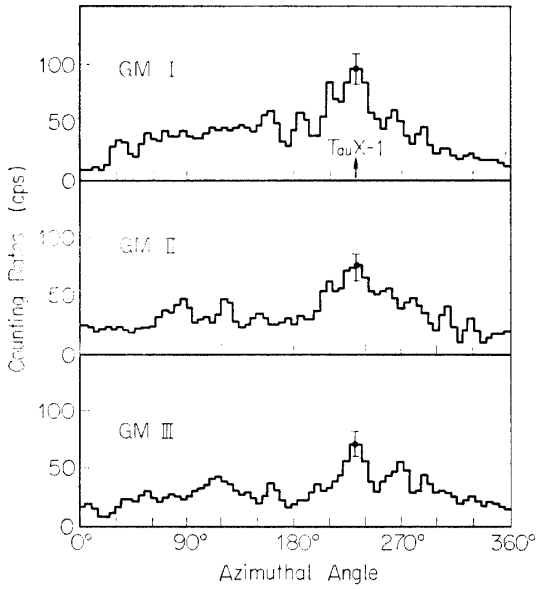

FIG. 24. Counting rates with respect to the rocket spin angle in GX-3.

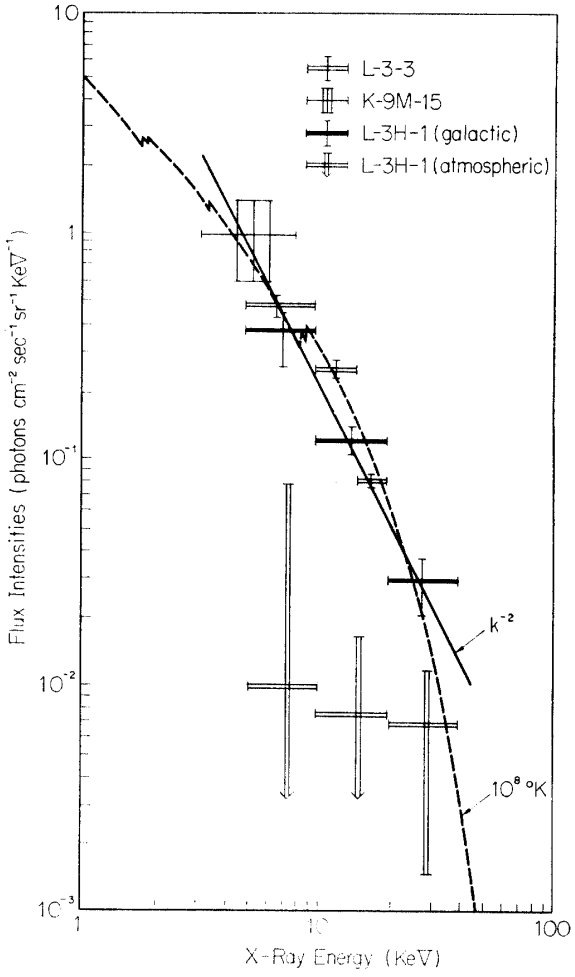

FIG. 25. Energy spectra of the isotropic component of galactic X-rays and of the atmospheric X-rays. The dashed curve in the figure represents a thermal spectrum at 10^8°K due to free-free and free-bound transitions, and the solid straight line represents a differential power spectrum.

were mounted on the second stage of L-3H-1 rocket, one parallel and the other perpendicular to the rocket axis, so that the former could observe X-rays from space and the latter both from space and the atmosphere.

Fig. 26 shows preliminary results of energy spectra of X-ray sources; Sco X-1, Cyg X-1 and Tau X-1. Results of other groups compared seem to be in fair agreement with each other. Although our data are preliminary especially for the absolute flux intensity, because accurate information on the rocket attitude is not available yet, our spectra indicate that the properties of X-ray sources of Sco X-1, Cyg X-1 and Tau X-1 would not be the same.

More detailed preliminary results of the flux intensities and energy spectra of galactic X-rays were reported in previous papers [*2*, *3*, *4*, *9*]. Results of more

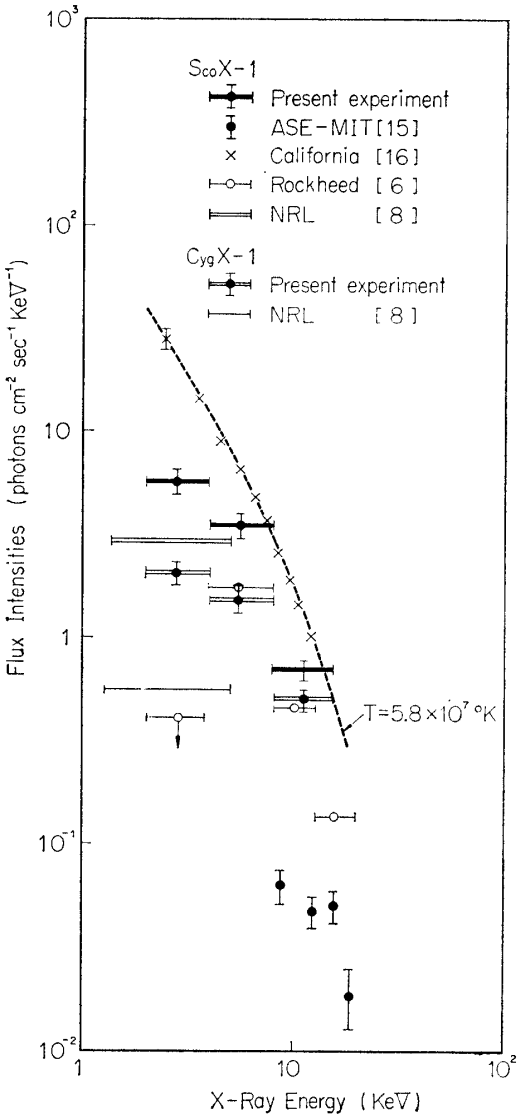

(a) Sco X-1 and Cyg X-1. The dotted curve in the figure represents a thermal spectrum at 5.8×10^{7}°K due to free-free transitions. Absolute intensities of our data are lower limits and those obtained by Rockheed and NRL groups are uncorrected.

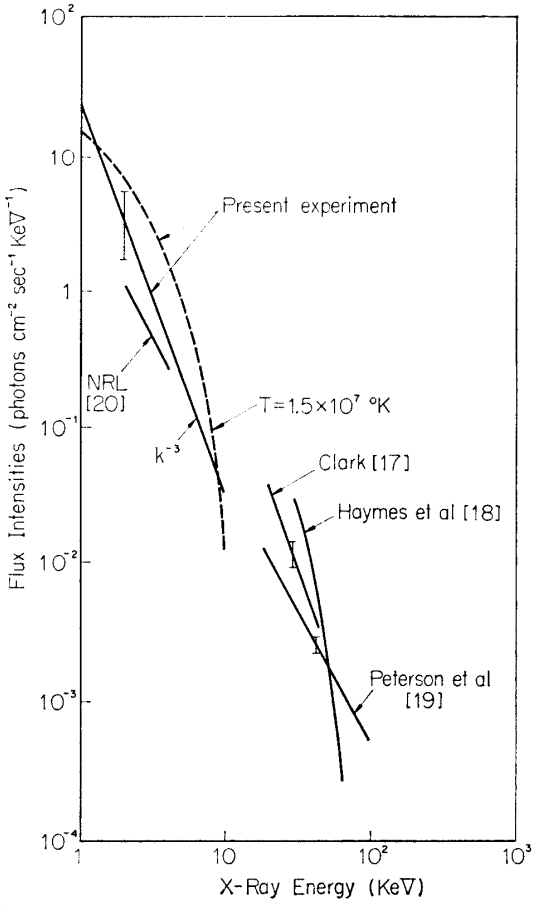

(b) Tau X-1. Absolute intensities of our data are lower limits. It is shown the best fits of spectral shapes deduced from our data.

FIG. 26. Energy spectra of galactic X-ray sources.

advanced analyses for galactic X-rays, albedo X-rays and charged particles will be published in separate papers.

7. ACKNOWLEDGEMENTS

The author wishes to express his hearty gratitudes to Professor S. Hayakawa of Nagoya University for suggesting this work and for his valuable advice and discussions, and to Drs. F. Makino and D. Sugimoto of Nagoya University for their helpful advice. He also wants to thank his co-workers, Messrs. K. Yamashita, H.

Ogawa and S. Yoshioka of Nagoya University for their helpful assistance.

Author's gratitudes are due also to Drs. Y. Miyazaki and H. Takeuchi of the Institute of Physics and Chemical Research, and to Professors A. Tamaki T. Nomura and K. Hirao of University of Tokyo for their kind advice and encouragement given this work.

The aid of Dr. T. Kurashige and Messrs. S. Urimoto, M. Koike, T. Ikehata and S. Koga of Meisei Electric Co., Ltd. for manufacture of instruments, and also the aid of Messrs. N. Mochida and A. Ishimura of Japan Radio Co., Ltd. for manufacture of gas counters are gratefully acknowledged.

Rocket flight services were provided by Institute of Space and Aeronautical Science, University of Tokyo and admirable teamwork of many people resulted in this work successfully.

Department of Space Science
Institute of Space and Aeronautical Science
University of Tokyo, Tokyo
May 11, 1966

References

[1] R. Giacconi, H. Gursky, F. Paolini and B. Rossi: Phys. Rev. Letters, **9** (1962), 439.
[2] S. Hayakawa, M. Matsuoka and K. Yamashita: Proc. of 6th COSPAR Symp. at Mar del Plata, 1965 (in press).
[3] S. Hayakawa, M. Matsuoka and K. Yamashita: Proc. of 9th International Conf. on Cosmic Rays at London, 1965 (in press).
[4] S. Hayakawa, M. Matsuoka, H. Ogawa and K. Yamashita: Proc. of 7th COSPAR Symp. at Vienna, May 1965 (to be published).
[5] G. Clark, G. Garmire, M. Oda, M. Wada, R. Giacconi, H. Gursky and J. R. Waters: Nature, **207** (1965), 584.
[6] P. C. Fisher, H. M. Johnson, W. C. Jordan, A. J. Meyerott and L. W. Acton: Astrophys. J., **143** (1966), 203.
[7] E. T. Byram, T. A. Chubb and H. Friedman: pre-print.
[8] S. Bowyer, E. T. Byram, T. A. Chubb and H. Friedman: Science, **147** (1965), 394.
[9] S. Bowyer, E. T. Byram, T. A. Chubb and H. Friedman: Science, **146** (1964), 912.
[10] M. Oda, G. Clark, G. Garmire, M. Wada, R. Giacconi, H. Gursky and J. Waters: Nature, **205** (1965), 554.
[11] S. Hayakawa, M. Matsuoka and D. Sugimoto: Space Science Reviews, **5** (1966), 109.
[12] R. L. F. Boyd: Space Science Reviews, **4** (1965), 35.
[13] D. Engelkemeir: Rev. Sci. Instr. **28** (1956), 589.
[14] R. Kajikawa, F. Makino, M. Matsuoka and Y. Tanaka: Jap. J. Apl. Phys., **3** (1961), 724.
[15] M. Oda: Proc. of 9th International Conf. on Cosmic Rays at London, 1965 (in press).
[16] G. Chodil, R. C. Topson, Hans Mark, F. D. Seward and C. D. Swift: Phys. Rev. Letters, **15** (1965), 605.
[17] G. W. Clark: Phys. Rev. Letters, **14** (1965), 91.
[18] R. C. Haymes and W. L. Graddak: Phys. Rev. Letters (in press).
[19] L. E. Peterson, A. S. Jacobson and R. M. Pelling: Phys. Rev. Letters, **16** (1966), 142.
[20] S. Bowyer et al.: cited in reference [17].